Available online at www.sciencedirect.com

ScienceDirect

Journal of Magnesium and Alloys 1 (2013) 283–291
www.elsevier.com/journals/journal-of-magnesium-and-alloys/2213-9567

Full length article

Microstructure and mechanical properties of a high ductility Mg–Zn–Mn–Ce magnesium alloy

Lei Gao [a,*], Hong Yan [b], Jun Luo [b], Alan A. Luo [c], Rongshi Chen [b]

[a] *General Motors China Science Lab, 56 Jinwan Road, Pudong, Shanghai 201206, China*
[b] *State Key Laboratory for Corrosion and Protections, Institute of Metal Research, Chinese Academy of Sciences, 62 Wencui Road, Shenyang 110016, Liaoning, China*
[c] *College of Engineering, The Ohio State University, Columbus, OH 43210, USA*

Received 24 October 2013; accepted 14 November 2013

Abstract

A high-ductility ZME200 (Mg–2.3Zn–0.4Mn–0.2Ce[1]) alloy was newly developed for vehicle closure and structure applications, based on an earlier ZE20 (Mg–2.0Zn–0.2Ce) alloy for extrusion applications. Previous study indicates that the hot deformation behavior of as-cast ZME200 alloy varies with processing parameters, namely temperature and strain rate. In this follow-up study, a conventional rolling process was optimized to obtain magnesium sheets with a very fine grain structure and high ductility. The microstructure, mechanical properties, and corrosion resistances of ZME200 alloy were investigated, and compared with those of commercial AZ31 magnesium alloy. It was demonstrated that the ZME200 alloy sheet exhibits extraordinarily higher ductility (36% in tensile elongation), much superior stretch formability (an Erichsen value of 9.5), lower anisotropy, comparable strength and corrosion resistance to AZ31 alloy. The unique RD–TD double split texture with remarkably reduced intensity and grain refinement gives rise to the significantly improved ductility and formability at room-temperature.

Keywords: Magnesium sheet; Mg–Zn–Mn–Ce; Ductility; Texture

1. Introduction

The low density, high specific strength and stiffness of wrought magnesium alloys make them attractive to the automotive industry for vehicle lightweighting. Recently, there have been many attempts to develop vehicle closures and structures, such as door inner panel, reinforcement, hood and decklid inner panel [1,2] by using AZ31 (Mg–3Al–1Zn–0.4Mn), the most commonly available rolled Mg sheet alloy. This alloy exhibits poor ductility, limited formability and strong anisotropy at ambient temperatures, while significantly high formability was obtained at elevated temperatures (>225 °C) [2]. This is the reason that magnesium sheet components are usually formed at elevated temperatures using processes such as superplastic forming, quick plastic forming or warm stamping [1]. It was reported that GM developed a production-ready magnesium rear decklid inner panel using quick plastic forming of AZ31 alloy and is the first to use thermal-formed magnesium sheet metal in structural applications [2]. However, warm forming processes are still expensive due to their long cycle time and heated toolings. It is expected magnesium sheet applications to grow with additional materials and process improvements targeted at reducing cost. Therefore, it is necessary to develop high

* Corresponding author. Tel.: +86 21 28987160; fax: +86 21 58321165.
E-mail addresses: lgao@alum.imr.ac.cn, lei.gao@gm.com (L. Gao).
Peer review under responsibility of National Engineering Research Center for Magnesium Alloys of China, Chongqing University

Production and hosting by Elsevier

[1] All compositions in wt.% except otherwise stated.

http://dx.doi.org/10.1016/j.jma.2013.11.005

Table 1
Chemical compositions of experimental ZME200 and commercial AZ31 alloys.

Alloy	Al	Zn	Mn	Ce	Mg
ZME200	–	2.26	0.38	0.23	Bal.
AZ31	3.1	1.1	0.42	–	Bal.

formability magnesium sheets capable of room temperature or near room temperature stamping, which could significantly reduce the cycle time and manufacturing costs.

A critical challenge for improving formability is tailoring the texture and grain size by alloy design and/or process optimization. In this study, ZME200 alloy was designed since Zn is added for strengthening, Ce for texture modification and Mn for corrosion resistance based on previous investigation [3,4]. This work examines the effects of rolling parameters, namely temperature and strain rate, on microstructure development of ZME200 magnesium alloy in the sheet condition, and their consequent effects on the mechanical properties and corrosion resistance of the alloy. The results were compared with those of commercial AZ31 alloy.

2. Experimental procedures

2.1. Alloy preparation and casting

The ZME200 alloy was prepared using commercial, high-purity magnesium (>99.95%), zinc (>99.9%), and Mg–30Ce and Mg–11Mn mater alloys by melting in an electric resistance furnace at about 780 °C under protection of anti-oxidizing flux. Billets with the dimensions of 150 mm × 200 mm × 200 mm were cast by pouring the melt at about 720 °C into a mild steel mold preheated to 200–300 °C. The actual chemical composition of the alloy was determined using inductively coupled plasma atomic emission spectroscopy (ICP-AES), and is listed in Table 1.

Table 2
Rolling process parameters for ZME200 alloy.

Specimen	Temperature (°C)	Reduction per pass (%)	Passes	Annealing
A	420	30	9	320 °C/30 min
B	320	30	9	320 °C/30 min
C	420	15	12	320 °C/30 min
D	320	15	12	320 °C/30 min

Commercial AZ31 alloy sheets with a thickness of ~1.5 mm were received in as-rolled condition (F temper) and used for comparison. The actual chemical composition is also listed in Table 1.

2.2. Hot rolling procedure

Rolling slabs with an initial thickness of ~20 mm were prepared and homogenized at a temperature of 400 °C for 10 h prior to rolling. The rolling experiments were performed with a speed of approximately 16 m/min (with the roll diameter of 350 mm and the width of 500 mm) and without the use of lubrication. In order to improve their rollability, original slabs were hot-rolled at 450 °C to 7 mm thickness with a 15% reduction per pass. Many edge cracks were observed due to the initial coarse grain size of the as-cast ingots [3]. Four ZME200 sheet specimens, A, B, C and D, were further rolled to sheets with a final thickness of 2.5 mm at 420 or 320 °C.

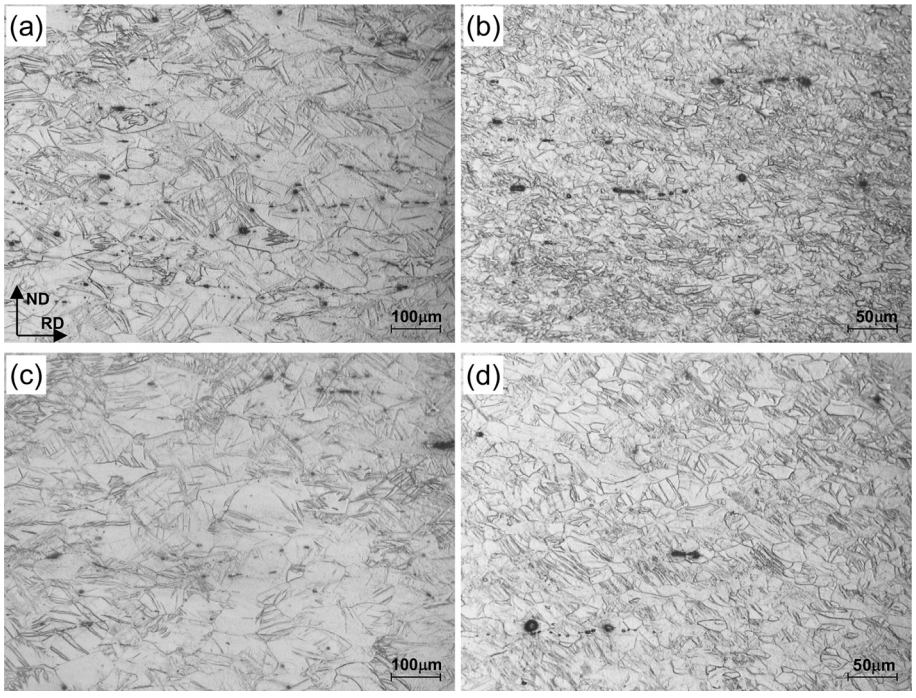

Fig. 1. Optical micrographs of the as-rolled ZME200 alloy in the RD–ND plane: (a) specimen A, (b) specimen B, (c) specimen C, and (d) specimen D. Rolling direction is horizontal.

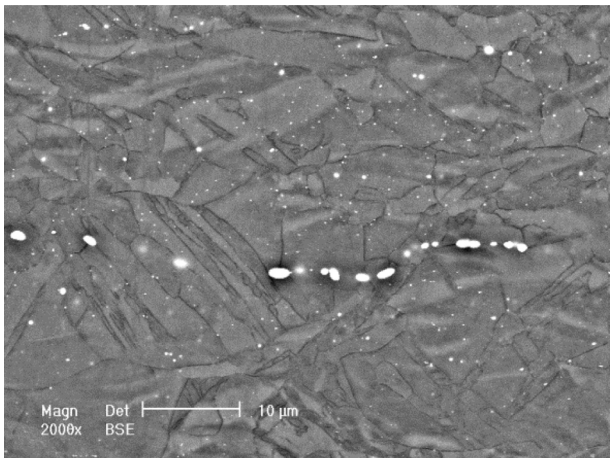

Fig. 2. SEM backscattered electron image of as-rolled specimen B showing deformation twinning and fine precipitates (light particles). Rolling direction is horizontal.

The rolling procedure, as shown in Table 2, consists of 9 or 12 passes with a constant thickness reduction of 30% or 15%, each referring to a true strain [5]:

$$\varepsilon = -\ln(h_{n+1}/h_n) = 0.36 \text{ or } 0.16, \quad (1)$$

where n is the number of the pass and h_n is the sample thickness after pass n. After each pass, the specimens were reheated to 420 or 320 °C and held for 15–30 min to maintain a consistent rolling temperature. Subsequently, the rolled specimens were annealed at 320 °C for 30 min to promote full or partial recrystallization.

2.3. Microstructure characterization

All microstructural and texture analyses were conducted on the mid-layer of the sheet samples. The specimens for optical microscopy (OM) and scanning electron microscopy (SEM) were polished to a mirror finish and then etched using a solution of 150 ml of water, 1 g of oxalic acid, 1 ml of nitric acid, and 1 ml acetic acid for 10–15 s. The average grain size (d) was determined using the mean linear intercept method, where $d = 1.74L$; and L is the linear intercept size. Texture analysis of the samples in the RD–TD plane was performed using the Schultz reflection method on a D8 DISCOVER Diffractometer. Calculated pole figures were obtained using the DIFFRAC plus TEXEVAl software and measured incomplete {0002}, {10–10} and {10–11} pole figures.

2.4. Mechanical and corrosion characterization

Uniaxial tensile specimens with a 15 mm gage length, a 3.5 mm gage width and a 2 mm gage thickness were machined from the sheets in three orientations: rolling direction (RD), 45° to RD and transverse direction (TD). The tensile tests were conducted at room temperature with an initial strain rate of 10^{-3} s^{-1}; and the on-sample strains were measured using an extensometer with a gage length of 10 mm. The true stress–strain (σ_T–ε_T) curves were derived from the nominal stress–strain (σ_N–ε_N) curves obtained in compression according to the following equations:

$$\sigma_T = \sigma_N(1 + \varepsilon_N), \varepsilon_T = \ln(1 + \varepsilon_N).$$

Circular blanks of 100 mm diameter were machined from the annealed specimens for the Erichsen tests to investigate the stretch formability of the ZME200 sheets at room temperature. The tests were carried out using a hemispherical shape punch of 50 mm diameter with a Teflon lubricant. The punch speed and blank-holder force were 20 mm/s and 25 kN, respectively.

Corrosion rates were measured using immersion tests at room temperature in a 3.5% NaCl solution for 72 h. The hydrogen evolved during the corrosion experiments was collected in a burette above the test samples. Post-immersion samples were cleaned chemically in a chromic acid solution (200 g/L CrO_3 and 10 g/L $AgNO_3$) for 5–10 min to remove the corrosion products.

3. Results and discussion

3.1. Microstructure of the rolled sheets

The microstructures of the as-rolled ZME200 alloy in the RD–ND plane are shown in Fig. 1, where ND is normal direction. A deformed microstructure with grains that are partly elongated along the rolling direction is observed as a result of the complex rolling procedure, especially of the final rolling pass [6]. Compared with the as-cast microstructure with coarse grains of ~500 μm [3], the grains were significantly refined by recrystallization during the rolling process or during reheating between rolling passes [7]. In the sheets rolled at a lower temperature (specimens B and D), the grains appear to be much smaller compared to that in the higher temperature rolled sheets (specimens A and C).

The as-rolled microstructures contain deformation heterogeneities with numerous twins and shear bands, which play an important role in the deformation process and the resulting microstructure during hot rolling. The density of twins and shear bands appears to be higher as the temperature decreases and the strain rate increases, which agrees well with an earlier observation during hot compression Gleeble tests [3]. Thus, specimen B has the highest twin density, and the twins are approximately 45° to the rolling direction. As also shown in SEM in Fig. 2, a large number of tiny particles (<1 μm) and fragmented Mg–Zn–Ce intermetallic compounds (1–2 μm) are precipitated within the matrix.

3.2. Microstructure of the annealed sheets

The microstructures of the annealed ZME200 alloy in the RD–ND plane are shown in Fig. 3. As expected, all specimens were partially recrystallized after annealing and equiaxed and fine grains were obtained. Twins were mostly distinguished and transformed to recrystallized grains due to the large strain energy stored in twins, which can apparently provide driving force for recrystallization [8]. However, some twins were also

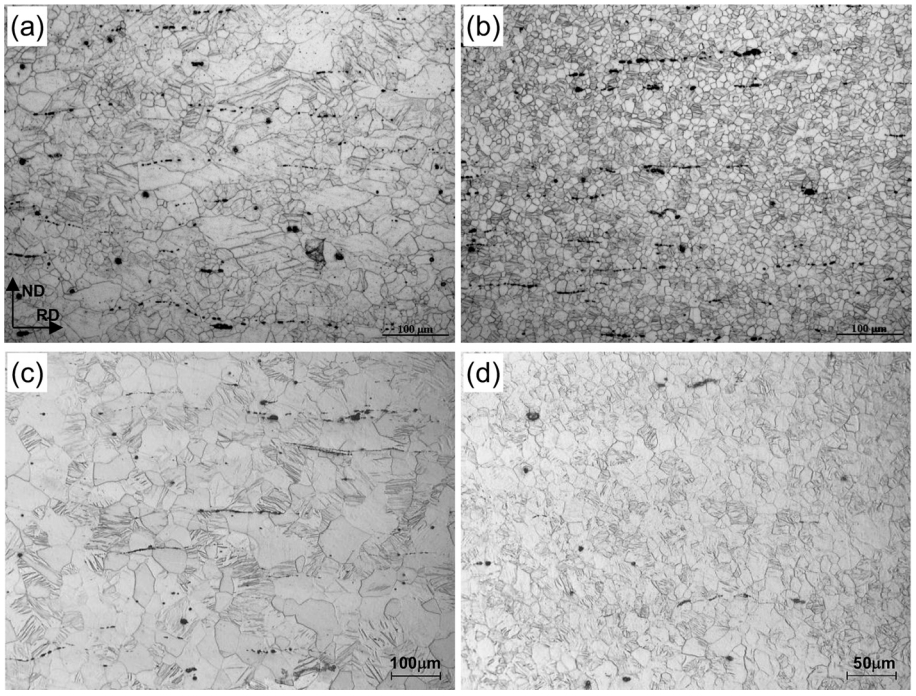

Fig. 3. Optical micrographs of the annealed ZME200 alloy in the RD–ND plane: (a) specimen A, (b) specimen B, (c) specimen C, and (d) specimen D. RD is horizontal.

residual, especially in specimens A and C, which may be attributed to the lower annealing temperature (320 °C) than the rolling temperature (420 °C). Additionally, it was reported that the addition of small amount of rare earth impeded recrystallization during rolling and annealing process [9], which is in contrast to the fact that AZ31 alloy generally showed equiaxed grain structures without twins [10].

The average grain sizes were 53, 17, 58, and 23 μm for specimens A–D, respectively. It is clear that the size of the recrystallized grains is affect by the processing parameters, i.e. strain rate (thickness reduction per pass) and deformation temperature. Additionally, the average grain size is more sensitive to the process temperature than to the strain rate. The relationship is usually expressed in terms of a temperature compensated strain rate parameter called Zener–Hollomon parameter ($Z = \dot{\varepsilon}\exp(Q/RT)$) [11], where $\dot{\varepsilon}$ is the strain rate, Q is the activation energy for dominant diffusion, T is the deformation temperature, and R is the gas constant. Specimen B exhibits the smallest grain size among the four samples, which is due to the more severe deformation at the lower rolling temperature. New grains nucleate at the original grain boundaries, while at the high Z parameter, there is an enhanced activity of deformation twinning, and new grains also nucleate at the twin interfaces [3].

3.3. Texture evolution

The (0002) pole figures of the as-rolled ZME200 alloy are shown in Fig. 4, where data of AZ31 is also included for comparison. It can be seen that the rolled AZ31 sheet sample exhibits a strong basal texture (8.54 in peak intensity in Fig. 4e) where the *c*-axes of the grains in the sheet are predominantly normal to the sheet surface. Such strong basal texture can also be found in some trace Gd alloying magnesium sheet alloys, like Mg–Zn–0.1Gd [12]. However, the ZME200 sheets show a weak (from 3.15 to 7.89 in peak intensity) and random basal texture (Fig. 5a–d) with broader distribution of basal poles towards TD that is similar to the texture in the RE-containing alloys [5,13]. Note that the texture intensity was sensitive to the variation in processing parameters. The lower the Zener–Hollomon parameter is, the weaker the texture intensity is. Following annealing, the texture of ZME200 is even weaker (2.35–3.20 in peak intensity), as shown in the (0002) pole figures in Fig. 5. It is interesting that specimen B exhibits the strongest texture intensity, which subsequently transferred to the lowest by recrystallization during annealing.

Also, the texture transformed from basal in the as-rolled state to non-basal in the as-annealed state, due to the grain orientation rotation caused by static recrystallization during the annealing process. Generally, a TD split, double peaks in the (0002) pole figure are obtained in specimens A, C, and D. However, an RD–TD double split, as in Fig. 5b, namely four distinct peaks in the (0002) pole figure, is observed in specimen B. Although recrystallization is very limited in the as-rolled conditions, on close examination, small recrystallized grains are actually distributed along shear bands or twins in all the specimens. These grains are assumed to have a texture tilted to RD, which is retained during annealing. Additionally, the annealed recrystallized grains evolve to the texture titled to TD. Therefore, the final texture evolved into a four peaks non-

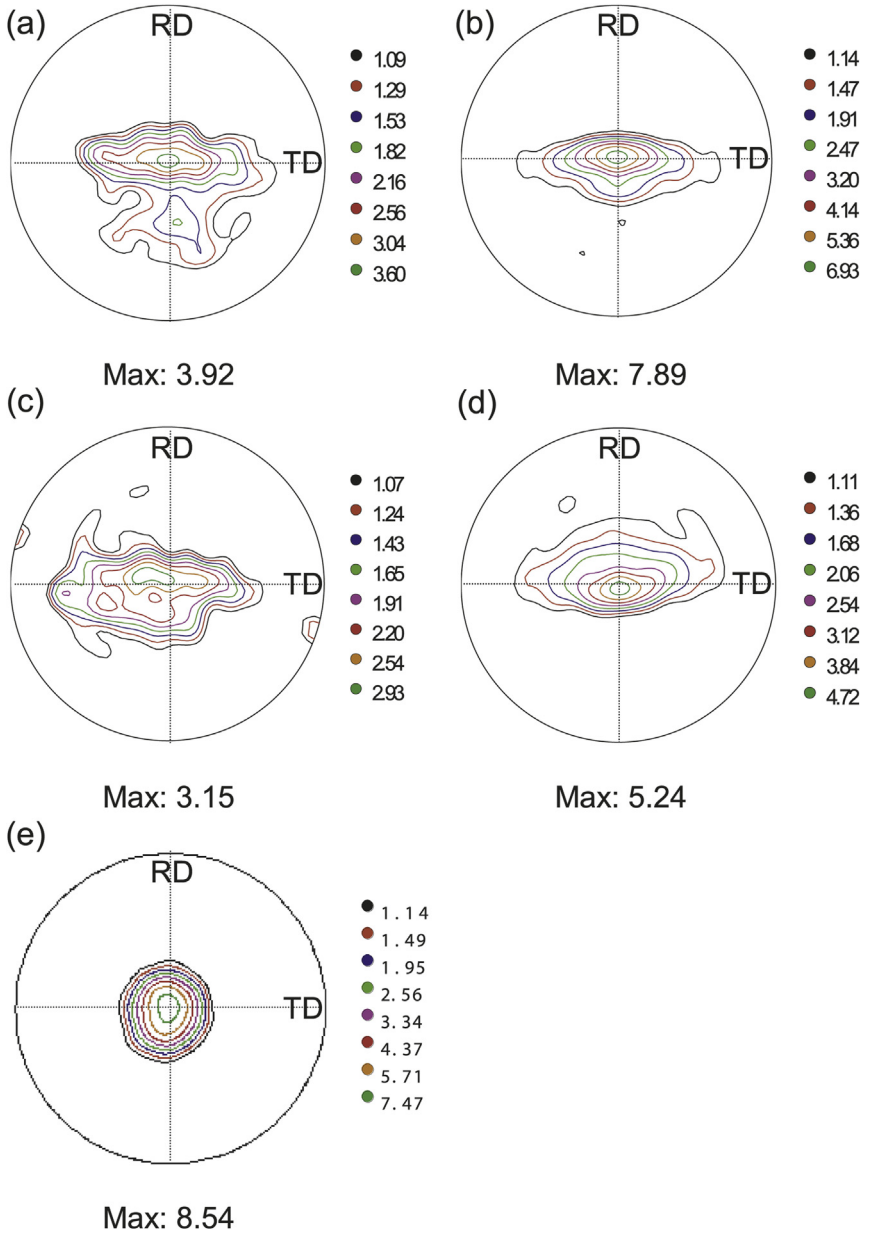

Fig. 4. (0002) pole figures of the as-rolled ZME200 and AZ31 alloys: (a) specimen A, (b) specimen B, (c) specimen C, (d) specimen D, and (e) AZ31.

basal texture. This was previously reported in rolled and partially recrystallized ZE10 sheet specimens [7], but not for the studied specimens A, C, and D. Further investigations are needed to understand the texture evolution mechanisms by annealing.

3.4. Mechanical properties and anisotropy

Typical engineering stress–strain curves of the as-rolled (F) and annealed (O) ZME200 sheets in the tensile direction of RD are shown in Fig. 6. The corresponding mechanical properties are listed in Table 3. It can be seen that the rolled sheets show higher yield strength and lower elongation due to the strong basal texture compared to the annealed state with a weakened non-basal texture. The annealed sheets show higher tensile elongation ranging from 25% to 38%, compared to less than 23% elongation of AZ31 alloy [14]. Specimen B in the annealed condition showed a tensile yield strength (YS) of approximately 143 MPa, with an ultimate tensile strength (UTS) of 236 MPa, with a tensile strain to failure (EL_f) of approximately 36.2%.

The yield strength, ultimate tensile strength, elongation to failure and uniform elongation in the tensile directions of RD, 45° and TD, are summarized in Table 3 and shown in Fig. 7, where θ is the angle between the rolling direction and the tensile direction. Specimens A, C, and D exhibit a yield anisotropy (Fig. 9a) typical of conventional magnesium alloys [5], such as AZ31 [15]. The highest yield strength is measured

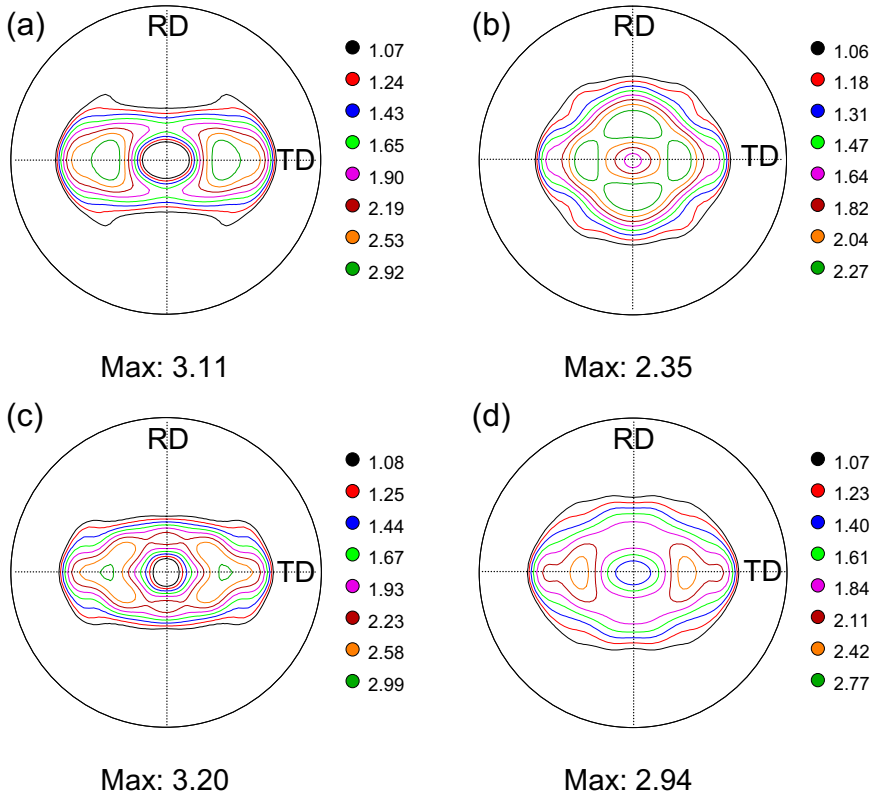

Fig. 5. (0002) pole figures of the annealed ZME200 alloy: (a) specimen A, (b) specimen B, (c) specimen C, and (d) specimen D.

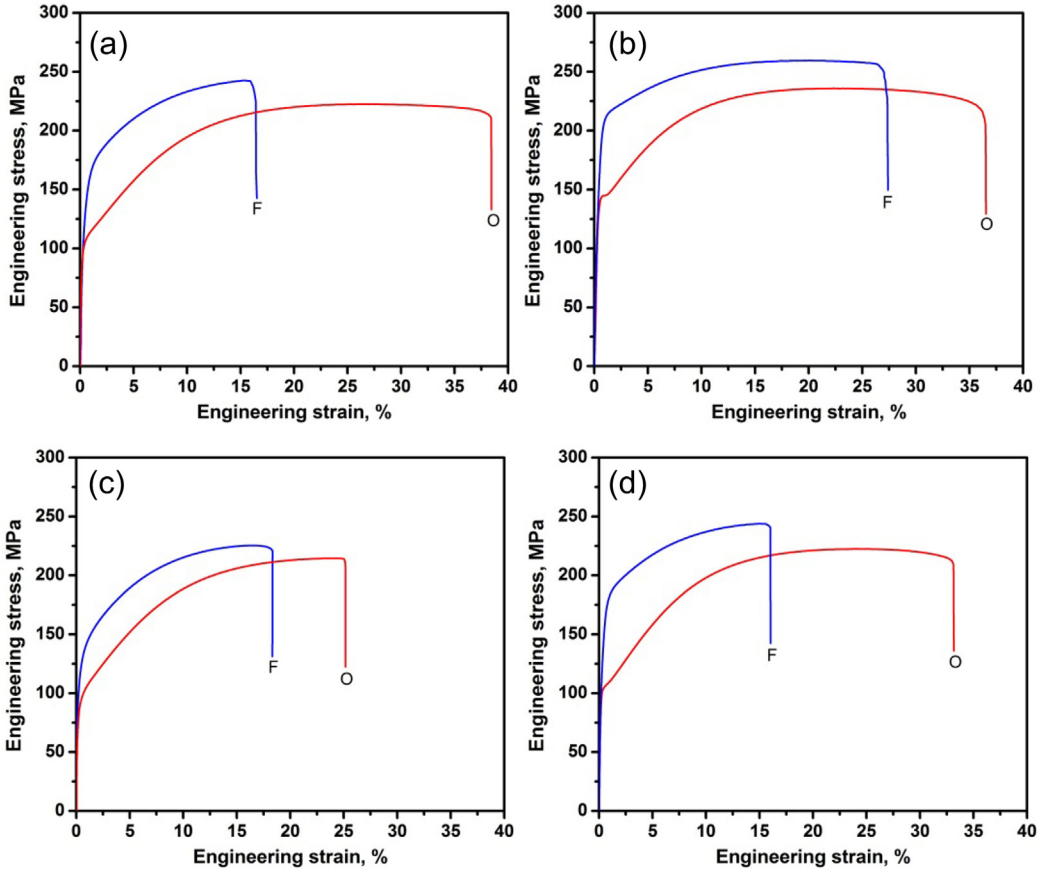

Fig. 6. Engineering stress−strain curves of the as-rolled (F) and annealed (O) ZME200 sheets along the rolling direction: (a) specimen A, (b) specimen B, (c) specimen C, and (d) specimen D.

Table 3
Tensile properties parallel to the rolling direction of ZME200 sheets (UTS, ultimate tensile strength; YS, 0.2% yield strength; EL_f, elongation to failure; EL_u, uniform elongation and n, n-value).

Sheet	Temper	Grain size/μm	Orientation	UTS/MPa	YS/MPa	EL_f/%	EL_u/%	n
A	F		RD	243	123	16.3	–	–
	O	53	RD	223	101	38.3	22.5	0.227
			45°	220	101	39.8	21.7	0.238
			TD	230	142	29.1	15.7	0.153
B	F		RD	260	168	27.1	–	–
	O	17	RD	236	143	36.2	19.0	0.188
			45°	237	148	34.1	19.2	0.202
			TD	238	148	36.5	18.5	0.175
C	F		RD	225	108	18.2	–	–
	O	58	RD	215	88	25	20.6	0.209
			45°	214	96	31.3	22.2	0.219
			TD	226	126	32.5	17.3	0.175
D	F		RD	244	131	15.9	–	–
	O	23	RD	223	103	32.9	21.8	0.208
			45°	228	119	36.0	21.3	0.207
			TD	232	134	31.4	17.1	0.163

along the TD and the lowest along the RD. However, this is not the case for specimen B, which shows almost the same strengths and elongation along the three directions, indicating low planar anisotropy.

3.5. Stretch formability

The results of the Erichsen tests at room temperature are shown in Fig. 8 for both the AZ31 and ZME200 sheets. Compared with the AZ31 alloy rolled sheets which exhibit

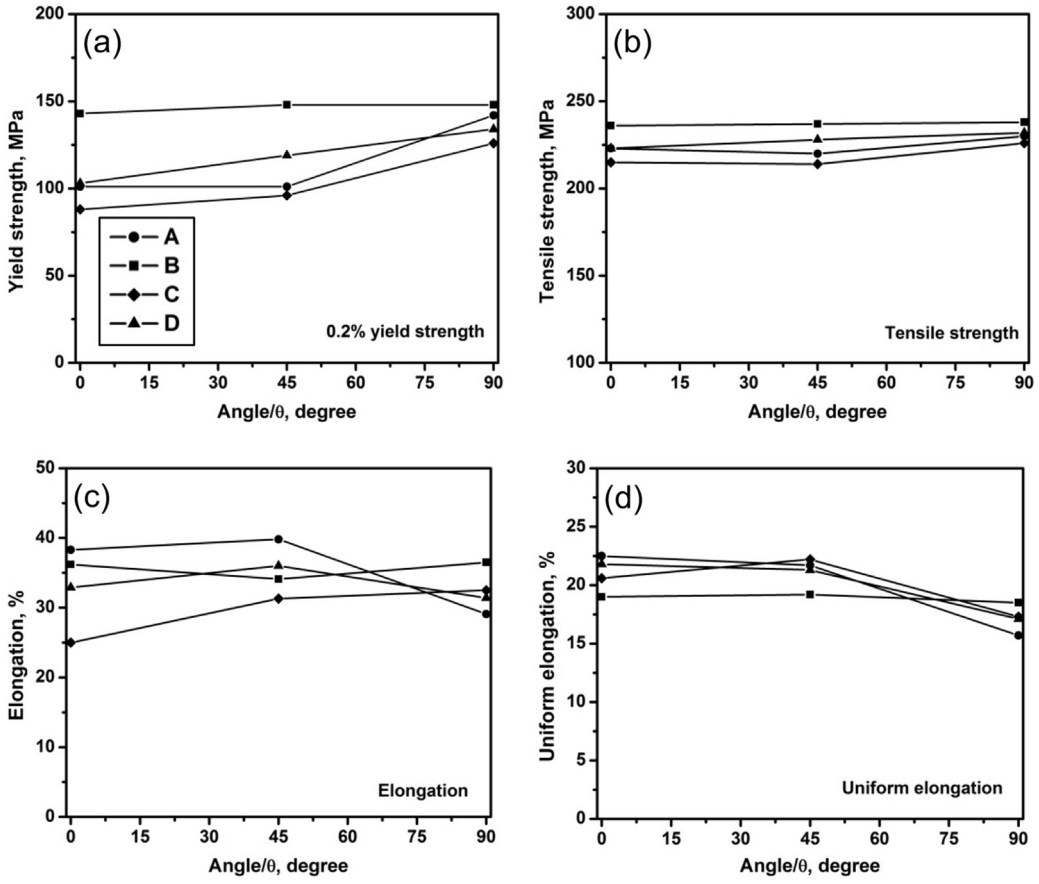

Fig. 7. Variation in 0.2% yield strength (a), tensile strength (b), elongation to failure (c) and uniform elongation (d) at room temperature as a function of the angle (θ) between RD and the tensile direction for specimens A–D.

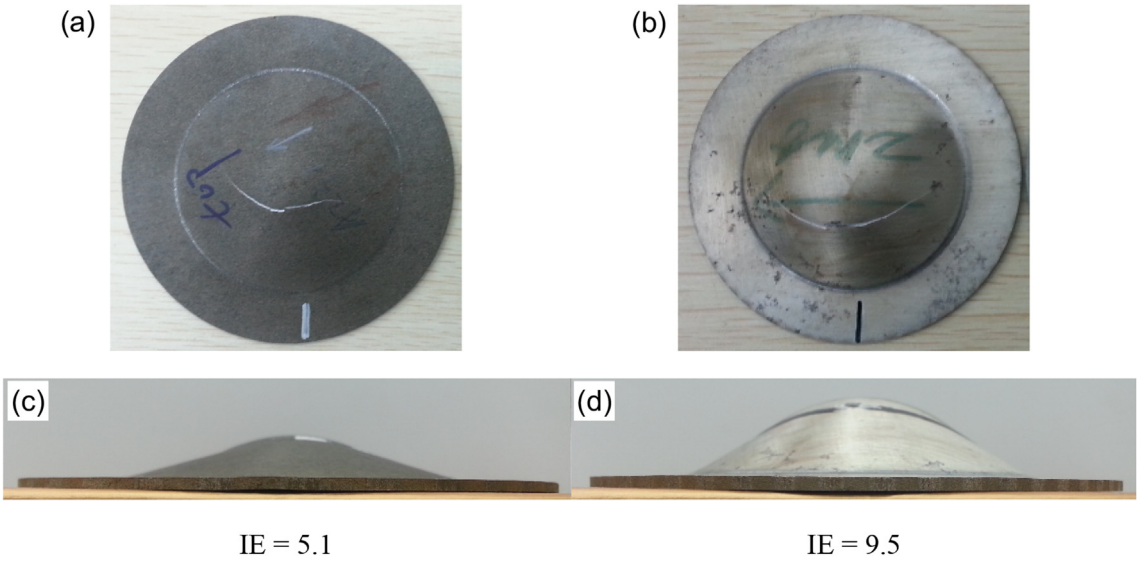

Fig. 8. Specimens and top view of the AZ31 (a and c) and ZME200 (b and d) sheets after the Erichsen tests at room temperature.

Erichsen values (IE) of 5.1 (Fig. 8(c)), the investigated ZME200 alloy sheet (specimen B) exhibits a superior stretch formability with an Erichsen value of 9.5 (Fig. 8(d)), which is almost the same as those of Al alloys [16]. Fig. 8(a) and (b) are the top view of the specimens after Erichsen tests. It reveals that the ZME200 alloy exhibits a surface crack parallel to the RD after Erichsen tests.

3.6. Corrosion behavior

The corrosion rates (a plot of the hydrogen evolution vs. immersion time) estimated from several repeated experiments of weight loss measurements for ZME200 are shown in Fig. 9, where data of AZ31 alloy has also been included for comparison. As 1 ml of H_2 evolution roughly corresponds to 1 mg of Mg dissolved [17], the plot shows that the corrosion rates of ZME200 alloys exhibited a decreasing trend with decreasing Z parameters, with specimen B of the highest corrosion rate (4.98 mm/year) and specimen C of the lowest corrosion rate (1.82 mm/year). A comparable corrosion rate was also noted for the ZME200 and AZ31 sheets. The H_2 evolution rates of all the sheets appeared nonlinear relative to the immersion time, i.e. faster at the beginning and gradually showing down as immersion time increased, indicating passivation [18]. The good corrosion performance of ZME200 alloys is probably attributed to the addition of Mn, which can improve the corrosion resistance by changing the Fe/Si impurities to the Mn–Si–Fe compound, as demonstrated in Fig. 10.

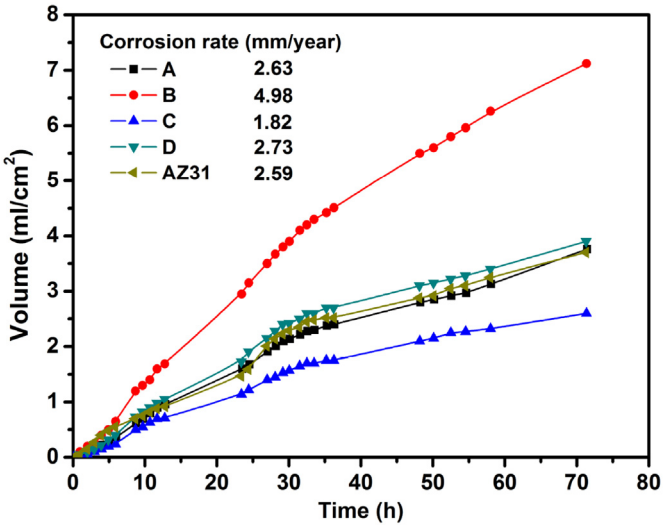

Fig. 9. Hydrogen evolution as a measure of corrosion rate of ZME200 alloys in 3.5% NaCl solution. All in the annealed condition (320 °C × 30 min).

4. Conclusions

The following conclusions can be drawn from the results in this work.

1) A new ZME200 (Mg–2.3Zn–0.4Mn–0.2Ce) magnesium alloy sheet has been developed using conventional hot rolling and subsequent annealing process. Compared with AZ31 Mg sheet, the ZME200 sheet shows extraordinarily higher ductility (36% in tensile elongation) and superior stretch formability (an Erichsen value of 9.5) and comparable strengths (143 MPa yield strength and 236 MPa ultimate tensile strength) and corrosion resistance (<5 mm/year in corrosion rate in 3.5% NaCl solution).
2) The rolling temperature and reduction per pass have great influences on the deformation mechanism and final microstructure of ZME200 alloy. Deformation twinning is more active at lower temperatures and higher thickness reductions, leading to finer microstructure. The texture formed in the as-rolled ZME200 alloy is a typical basal texture with wide spread to transverse direction (TD), and the intensity is lower than that of AZ31.
3) A non-basal texture in ZME200 alloy with double peaks spread to TD was formed due to static recrystallization during annealing. The peak intensity was further reduced

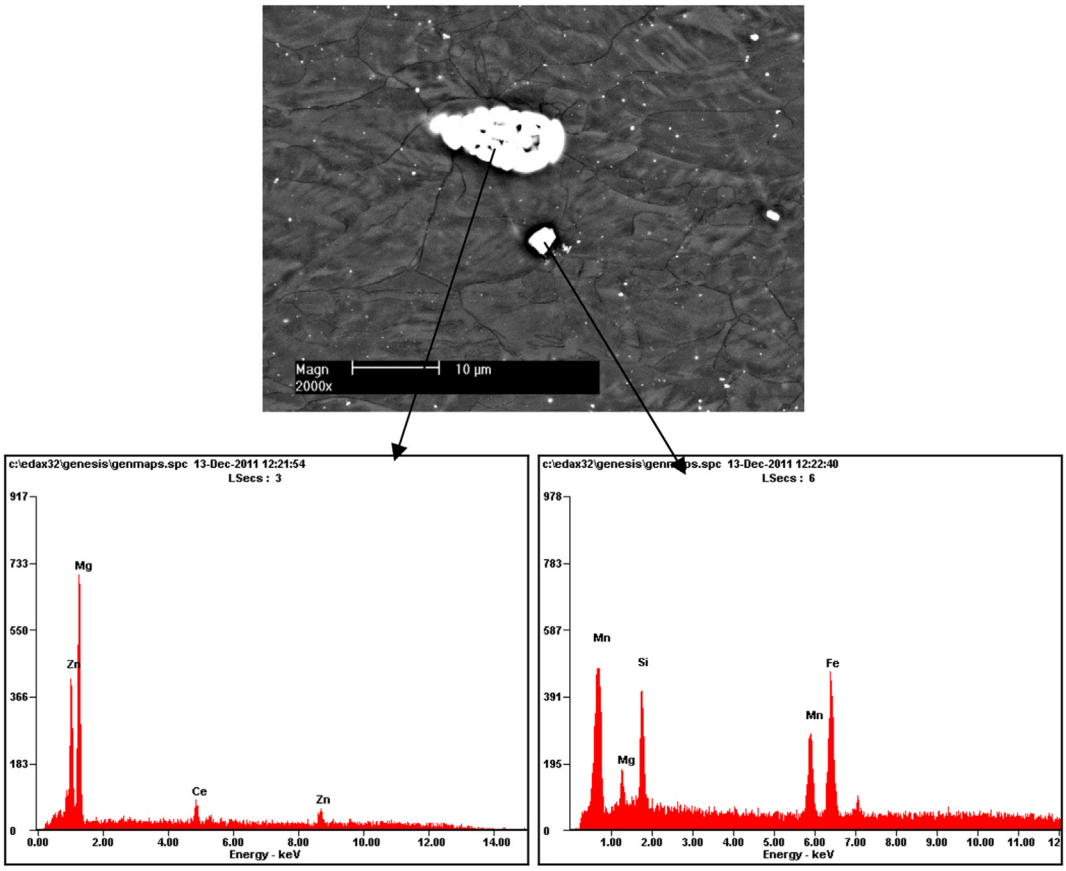

Fig. 10. SEM and EDS images of the as-rolled ZME200 alloy showing the Mn−Si−Fe and Mg−Zn−Ce compounds.

and the grain size was greatly refined by recrystallization during the annealing process. The significantly improved ductility and stretch formability of ZME200 alloy at room temperature is attributed to the transition of texture from a basal to a non-basal texture and the reduction of intensity, combined with grain refinement. Specimen B exhibits an unusual non-basal texture of RD−TD double split into four peaks, which eliminates the planar anisotropy.

Acknowledgments

This work was carried out as a collaborative research program supported by General Motors and Institute of Metal Research, Chinese Academy of Sciences. Prof. Xiaoqin Zeng and Shiyi Wang from Shanghai Jiaotong University and Prof. Jianping Lin and Ling Zhang from Tongji University are acknowledged for tensile and Erichsen tests. Drs. Jeff Wang, Jon Carter and Ming Liu from GM R&D are acknowledged for valuable discussion on sheet magnesium applications and corrosion, respectively.

References

[1] P.E. Krajewski, SAE Paper (2001) 2001-01-3104.
[2] R. Verma, J.T. Carter, SAE Paper (2006) 2006-01-0525.
[3] L. Gao, A.A. Luo, Mater. Sci. Eng. A 560 (2013) 492−499.
[4] A.A. Luo, R.K. Mishra, A.K. Sachdev, Script. Mater. 64 (2011) 410−413.
[5] J. Bohlen, M.R. Nurnberg, J.W. Senn, D. Letzig, S.R. Agnew, Acta Mater. 55 (2007) 2101−2112.
[6] K. Hantzsche, J. Bohlen, J. Wendt, K.U. Kainer, S.B. Yi, D. Letzig, Script. Mater. 63 (2010) 725−730.
[7] L.W.F. Mackenzie, M.O. Pekguleryuz, Script. Mater. 59 (2008) 665−668.
[8] S.Q. Zhu, H.G. Yan, J.H. Chen, Y.Z. Wu, J.Z. Liu, J. Tian, Script. Mater. 63 (2010) 985−988.
[9] H. Zhang, G. Huang, L. Wang, J. Li, Script. Mater. 67 (2012) 495−498.
[10] X. Huang, K. Suzuki, Y. Chino, M. Mabuchi, J. Alloy. Compd. 537 (2012) 80−86.
[11] C. Zener, J.H. Hollomon, J. Appl. Phys. 15 (1944) 22−27.
[12] H. Yan, R.S. Chen, N. Zheng, J. Luo, S. Kamado, E.H. Han, J. Magn. Alloy. 1 (2013) 23−30.
[13] Y. Chino, K. Sassa, M. Mabuchi, Mater. Sci. Eng. A 513−514 (2009) 394−400.
[14] H. Yan, R.S. Chen, E.H. Han, Mater. Sci. Eng. A 527 (2010) 3317−3322.
[15] F. Kaiser, J. Bohlen, D. Letzig, K.U. Kainer, A. Styczynski, C. Hartig, Adv. Eng. Mater 5 (2003) 891−896.
[16] Japan Light Metal Association (Ed.), Aluminum Handbook, Japan Light Metal Association, Tokyo, 2000, p. 98.
[17] G.L. Song, Adv. Eng. Mater 7 (2005) 563−586.
[18] W. Wen, A.A. Luo, T. Zhai, Y. Jin, Y.T. Cheng, I. Hoffmann, Script. Mater. 67 (2012) 879−882.